European Journal of Mechanics / A Solids 71 (2018) 320–325

Contents lists available at ScienceDirect

European Journal of Mechanics / A Solids

journal homepage: www.elsevier.com/locate/ejmsol

Modeling diffusion–induced stress on two-phase lithiation in lithium-ion batteries

Hui Wu[a], Zhoucan Xie[b], Yan Wang[c,d], Chunsheng Lu[d], Zengsheng Ma[a,*]

[a] National – Provincial Laboratory of Special Function Thin Film Materials, School of Materials Science and Engineering, Xiangtan University, Hunan, 411105, China
[b] State Key Laboratory of Nonlinear Mechanics, Institute of Mechanics, Chinese Academy of Science, Beijing, 100190, China
[c] School of Information and Electronic Engineering, Hunan University of Science and Technology, Hunan, 411201, China
[d] Department of Mechanical Engineering, Curtin University, Perth, WA, 6845, Australia

ARTICLE INFO

Keywords:
Lithium-ion battery
Two-phase lithiation
Fracture
Critical size

ABSTRACT

Capacity fade induced by chemo-mechanical degradation during charge-discharge cycles is the bottleneck in the design of high-performance batteries, especially high-capacity electrode materials. In this paper, a flexible sigmoid function is used to create the two-phase electrochemical lithiation profile, describing a sharp phase boundary that separates the pristine core from the lithiated shell of an electrode particle. According to such a phase transition, an analytical solution of the stress evolution is obtained by introducing an electrochemical reaction layer into the plastic model. Finally, based on the theory of diffusion-induced stress and the energy principle, we determine the critical thickness of radius of a lithiated layer, at which fracture occurs.

1. Introduction

Lithium-ion batteries (LIBs) have been widely used as power devices for portable electronics (Mukhopadhyay and Sheldon, 2014; Nam et al., 2006; Van Noorden, 2014). Silicon (Si) is emerging as the most promising anode material, given its theoretical capacity ten times high as that of conventional graphite-based anodes (Chen et al., 2014; Yao et al., 2011). As is known, a large volume swelling of ~300% during Li insertion (or extraction) may result in fracture of active Si anodes and irreversible capacity fading (Jia and Li, 2016). However, there is still not a good understanding on its intrinsic mechanism.

Recently, experimental observations have shown the formation of a core-shell structure in a partially lithiated Si nanoparticle, which consists of a two-phase boundary that separates an inner core of crystalline Si from an outer shell of amorphous Li_xSi ($x = 3.75$) (Liu et al., 2012; McDowell et al., 2012). A sharp phase boundary implies that the Li-poor and Li-rich phases do not transform continuously (McDowell et al., 2013). An abrupt change of Li concentration across the amorphous-crystalline interface promotes a drastic volume strain inhomogeneity, which is significantly different from that of single-phase lithiation (Wang et al., 2013). Thus, it is necessary to investigate the diffusion-induced stress, deformation and fracture on the basis of a two-phase electrochemical reaction lithiation process. In consideration of the analogy between diffusion and heat flow, diffusion-induced stress can be modeled as thermal stress (Lee et al., 2000; Prussin, 1961; Song et al., 2012; Yang, 2013; Yao et al., 2011). It is shown that there is a hoop compression stress in the surface layer and a tension stress in the center where fracture appears. However, this contrasts with *in situ* transmission electron microscopy observations of fracture initiation on the particle surface (Liu et al., 2012; McDowell et al., 2012).

During lithiation and delithiation processes, the lithiation-induced large deformation of Si electrodes is accommodated by plastic flow when stress exceeds the yield strength (Chon et al., 2011; Sethuraman et al., 2010). This makes it possible for Si anodes with small size to maintain a high capacity after many cycles, such as thin films (Takamura et al., 2004), nanowires (Chan et al., 2008), and porous structures (Wada et al., 2014). Sethuraman et al. (2010) measured the diffusion-induced stress as a function of the state of charge (SOC) in an amorphous Si thin film and found a pronounced hysteresis, indicating plastic deformation of lithiated Si. The microscopic mechanism was elucidated for the onset of large plastic deformation in lithiated crystalline Si (*c*-Si) and amorphous Si (*a*-Si) (Zhao et al., 2011), and captured the dramatic brittle-to-ductile transition of *a*-Si at a relatively low Li concentration by first-principles computational methods. A new stress-dependent chemical potential was reported for solid state diffusion under multiple driving forces (Cui et al., 2012), and also discovered that when plastic deformation occurs, the hoop stress is tensile on the particle surface.

On the other hand, the two-phase electrochemical reaction lithiation plays an important role in the stress evolution. A two-phase model

* Corresponding author.
E-mail address: zsma@xtu.edu.cn (Z. Ma).

https://doi.org/10.1016/j.euromechsol.2018.04.005
Received 17 May 2016; Received in revised form 31 March 2018; Accepted 9 April 2018
Available online 11 April 2018

was presented with the diffusivity dependence on Li concentration to describe the evolving core-shell structure with a sharp interface between Li-poor core and Li-rich shell (Liu et al., 2012). Also, anisotropic swelling and fracture of Si nanowires during lithiation were studied (Yang et al., 2012). An analytical solution of the co-evolving reaction and rigid-plasticity was exhibited in a spherical particle to explain the stress evolution (Zhao et al., 2012b). The kinetic model and finite element simulation were applied to obtain solutions of the Li-ion concentration distribution, the moving velocity of phase interface and the stress evolution (Pharr et al., 2012; Xie et al., 2016). A mechanics foundation was proposed for a direct physical understanding of stress generation during lithiation of high-capacity electrode materials with curved geometries (Huang et al., 2013).

In spite of the plastic flow and two-phase electrochemical lithiation, there is a strong size dependence of fracture, which means that, over a critical diameter, particles initially crack on surfaces and then fracture due to lithiation-induced swelling (Haftbaradaran and Gao, 2012; Liu et al., 2011, 2012; Zhao et al., 2010, 2012a). Using the theory of diffusion-induced stress and the energy principle, relations between the critical concentration of solute atoms and average damage size can be established for insertion-induced cracking and buckling in an elastic film (Yang, 2011). From the perspective of strain energy release rate, the critical size of various Si nanostructures can be also determined (Ma et al., 2013). Taking fracture and debonding of hollow core-shell nanostructures into account, the critical size was investigated relating to the core radius, the shell thickness, and SOC for a hollow structure (Ma et al., 2015; Zhao et al., 2012a).

In this paper, we aim to build up an analytical solution of diffusion-induced stress based on a two-phase lithiation process. The paper is organized as follows. In Section 2, a sigmoid function is set to be the analytical solution of concentration. Further, by introducing an elastic transition layer in an elastic-plastic model, the analytical relation between stress and radius of the elastic transition layer is obtained. In Section 3, the Li concentration profile, lithiated shell thickness, diffusion-induced stress field, and the size-dependent fracture are discussed. Finally, the concluding remarks are given in Section 4.

2. Theoretical model

2.1. Concentration

As illustrated in Fig. 1, the crystalline core (*c*-Si) is surrounded by an amorphous shell (*a*-Li_xSi) in a core-shell Si electrode. Initially, the electrochemical charge-transfer reaction at electrode-electrolyte interfaces causes Li-ions to be reduced with intercalation of Li in electrodes. Then, Li atoms diffuse through lithiated Si, and react with crystalline Si to form an amorphous phase at the reaction front. Here, migration of Li-ions in electrolyte is controlled by the Li diffusion through Li_xSi and the reaction of Li and Si at interface between Li_xSi and Si. According to previous studies (Xie et al., 2016; Zhao et al., 2012b), the relative rate of diffusion and reaction can be characterized as $\beta = D/kR$, where D is the diffusivity of Li in the lithiated Si, k is the velocity of the reaction front, and R is the particle size. If β is large, the diffusion of Li is fast,

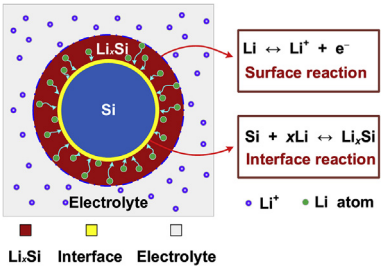

Fig. 1. Schematic illustration of the two-phase mechanism for Li-ion diffusion.

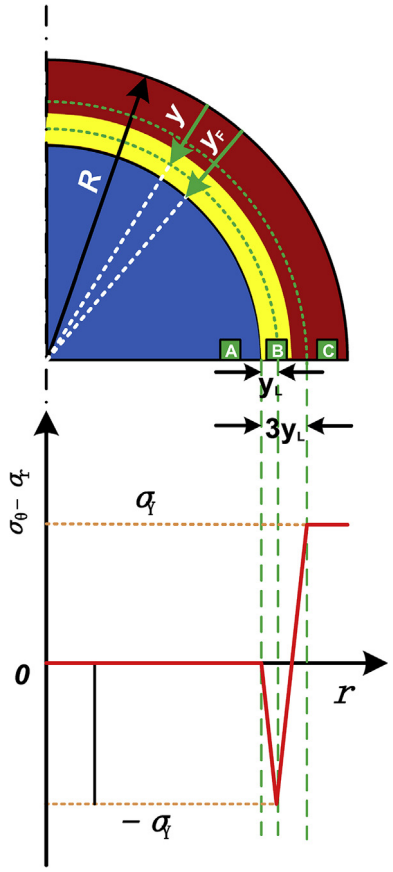

Fig. 2. Illustration of the stress state of a core-shell structure in a partially lithiated electrode particle.

and lithiation is limited by the electrochemical reaction. For the migration of phase boundaries, we adopt a flexible sigmoid (or generalized logistic (Huang et al., 2013)) function to describe the Li-ion concentration, $c(r)$ along the radius, r, that is

$$\frac{c(r)}{c_0} = \frac{1}{1 + \exp\left[-\beta\frac{r-(R-y)}{R}\right]} \tag{1}$$

where y is the center position between the two-phase boundary ($c = 0.5$) and surface. Such a logistic function in Eq. (1) has two asymptotic limits of $c = 0$ and 1, representing the pristine Si core and $Li_{3.75}Si$ shell, respectively. To move the phase boundary from the particle surface ($y = 0$) to its center ($y = R$), we can prescribe different time laws. As illustrated in Fig. 2, the transition layer thickness can be written as, $2y_L = 2(y_F - y)$, where y_F is the thickness of lithiation layer. Then, the SOC is deduced as

$$\mathrm{SOC} = \frac{\int_0^R c(r)r^2dr}{\int_0^R r^2dr} \approx \frac{R^3-(R-y)^3}{R^3} = 1-\left(1-\frac{y}{R}\right)^3 \tag{2}$$

2.2. Stress

In the case of a symmetrical spherical particle, the stress state can be represented by (σ_r, σ_θ, σ_θ), with σ_r and σ_θ the radial and hoop stresses, respectively. As shown in Fig. 2, the crystalline core is under homogeneous hydrostatic compression, so the stress state of element A is $\sigma_\theta - \sigma_r = 0$. On the two-phase boundary, as the reaction front sweeps through element B, a large lithiation strain creates at zone B. Owing to the constraint of surrounding materials, local compressive stresses reach to the yield stress σ_Y, viz. $\sigma_\theta - \sigma_r = -\sigma_Y$. The material element C is pushed outward by newly lithiated Si, causing further displacement

in the outward radial direction. Simultaneously, the hoop stress transfers from compression to tension in the shell. In addition, we assume that stress changes linearly with the thickness of translation layer. In the region of $y_F < r < y$, tensile stress decreases linearly to zero and then transfers to compression and increases to yield stress. In the region of $y < r < y + 2y_L$, it is just opposite.

At the beginning of lithiation, the crystalline core is in a state of homogeneous hydrostatic compression by the surface layer, so the stress state of element A is $\sigma_\theta - \sigma_r = 0$. When the thickness of lithiation layer is less than y_L, the stress state of rich-Li phase is

$$\sigma_\theta - \sigma_r = -\frac{\sigma_Y}{y_L}[r - (R - y_F)] \tag{3}$$

The balance of forces acting on an element requires that

$$\frac{d\sigma_r}{dr} + 2\frac{\sigma_\theta - \sigma_r}{r} = 0 \tag{4}$$

with the traction-free boundary condition, $\sigma_r|_{r=R} = 0$, and then we have

$$\sigma_r = 2\sigma_Y\left[\frac{R-r}{y_L} + \frac{R-y_F}{y_L}\ln\left[\frac{r}{R}\right]\right] \tag{5}$$

$$\sigma_\theta = 2\sigma_Y\left[\frac{3(R-r-2y_F)}{2y_L} + \frac{R-y_F}{y_L}\ln\left[\frac{r}{R}\right]\right] \tag{6}$$

The stress state at $0 \le r \le R - y_F$ is $\sigma_\theta - \sigma_r = 0$. Considering the continuous stress at phase boundary, $\sigma_r|_{r=(R-y_F)^+} = \sigma_r|_{r=(R-y_F)^-}$, we can obtain

$$\sigma_r = \sigma_\theta = 2\frac{\sigma_Y}{y_L}\left[y_F + (R-y_F)\ln\left[\frac{R-y_F}{R}\right]\right] \tag{7}$$

Similarly, with lithiation continuing, the stress state can be determined when the thickness of lithiation layer is larger than y_L and less than 3 y_L. The equivalent, radial and hoop stresses of electrode are as follows:

$$\sigma_\theta - \sigma_r = \begin{cases} -\sigma_Y\frac{r-R+(y_F-y_L)}{y_L}, & R-(y_F-y_L) < r \le R \\ -\sigma_Y\frac{r-R+y_F}{y_L}, & R-y_F \le r \le R-(y_F-y_L) \\ 0, & r \le R-y_F \end{cases} \tag{8}$$

$$\sigma_r = \begin{cases} 2\sigma_Y\left[\frac{r-R}{y_L} - \frac{R-y_F+2y_L}{y_L}\ln\left[\frac{r}{R}\right]\right], & R-(y_F-y_L) < r \le R \\ 2\sigma_Y\left[\frac{R-r-2y_F+2y_L}{y_L} + \frac{R-y_F}{y_L}\ln\left[\frac{r}{R-y_F+y_L}\right] - \frac{R-y_F+2y_L}{y_L}\ln\left[\frac{R-y_F+y_L}{r}\right]\right], & R-y_F \le r \le R-(y_F-y_L) \\ 2\sigma_Y\left[\frac{2y_L-y_F}{y_L} + \frac{R-y_F}{y_L}\ln\left[\frac{R-y_F}{R-y_F+y_L}\right] - \frac{R-y_F+2y_L}{y_L}\ln\left[\frac{R-y_F+y_L}{R}\right]\right], & r \le R-y_F \end{cases} \tag{9}$$

$$\sigma_\theta = \begin{cases} 2\sigma_Y\left[\frac{3r-3R+y_F-y_L}{2y_L} - \frac{R-y_F+2y_L}{y_L}\ln\left[\frac{r}{R}\right]\right], & R-(y_F-y_L) < r \le R \\ 2\sigma_Y\left[\frac{R-r-5y_F+4y_L}{2y_L} + \frac{R-y_F}{y_L}\ln\left[\frac{r}{R-y_F+y_L}\right] - \frac{R-y_F+2y_L}{y_L}\ln\left[\frac{R-y_F+y_L}{R}\right]\right], & R-y_F \le r \le R-(y_F-y_L) \\ 2\sigma_Y\left[\frac{2y_L-y_F+(R-y_F)}{y_L}\ln\left[\frac{R-y_F}{R-y_F+y_L}\right] - \frac{R-y_F+2y_L}{y_L}\ln\left[\frac{R-y_F+y_L}{R}\right]\right], & r \le R-y_F \end{cases} \tag{10}$$

When the thickness of lithiation layer is larger than $3y_L$, the stress state can be deduced as

$$\sigma_\theta - \sigma_r = \begin{cases} \sigma_Y, & R-(y_F-3y_L) < r \le R \\ \sigma_Y\frac{r-R+(y_F-2y_L)}{y_L}, & R-(y_F-y_L) < r \le R-(y_F-3y_L) \\ -\sigma_Y\frac{r-R+y_F}{y_L}, & R-y_F \le r \le R-(y_F-y_L) \\ 0, & r \le R-y_F \end{cases} \tag{11}$$

$$\sigma_r = \begin{cases} -2\sigma_Y\ln\left[\frac{R}{r}\right], & R-(y_F-3y_L) < r \le R \\ 2\sigma_Y\left[\frac{r-R+(y_F-3y_L)}{y_L} - \frac{R-y_F+2y_L}{y_L}\ln\left[\frac{r}{R-y_F+3y_L}\right] + \ln\left[\frac{R-y_F+3y_L}{R}\right]\right], & R-(y_F-y_L) < r \le R-(y_F-3y_L) \\ 2\sigma_Y\left[\frac{R-r-(y_F+y_L)}{y_L} - \frac{R-y_F+2y_L}{y_L}\ln\left[\frac{R-y_F+y_L}{R-y_F+3y_L}\right] + \ln\left[\frac{R-y_F+3y_L}{R}\right] + \frac{R-y_F}{y_L}\ln\left[\frac{r}{R-y_F+y_L}\right]\right], & R-y_F \le r \le R-(y_F-y_L) \\ 2\sigma_Y\left[-1 - \frac{R-y_F+2y_L}{y_L}\ln\left[\frac{R-y_F+y_L}{R-y_F+3y_L}\right] + \ln\left[\frac{R-y_F+3y_L}{R}\right] + \frac{R-y_F}{y_L}\ln\left[\frac{R-y_F}{R-y_F+y_L}\right]\right], & r \le R-y_F \end{cases} \tag{12}$$

$$\sigma_\theta = \begin{cases} 2\sigma_Y\left[\frac{1}{2} - \ln\left[\frac{R}{r}\right]\right], & R-(y_F-3y_L) < r \le R \\ 2\sigma_Y\left[-4 + \frac{3(r-R+y_F)}{2y_L} - \frac{R-y_F+2y_L}{y_L}\ln\left[\frac{r}{R-y_F+3y_L}\right] + \ln\left[\frac{R-y_F+3y_L}{R}\right]\right], & R-(y_F-y_L) < r \le R-(y_F-3y_L) \\ 2\sigma_Y\left[\frac{3(R-r-y_F-y_L)}{2y_L} - \frac{R-y_F+2y_L}{y_L}\ln\left[\frac{R-y_F+y_L}{R-y_F+3y_L}\right] + \ln\left[\frac{R-y_F+3y_L}{R}\right] + \frac{R-y_F}{y_L}\ln\left[\frac{r}{R-y_F+y_L}\right]\right], & R-y_F \le r \le R-(y_F-y_L) \\ 2\sigma_Y\left[-\frac{3}{2} - \frac{R-y_F+2y_L}{y_L}\ln\left[\frac{R-y_F+y_L}{R-y_F+3y_L}\right] + \ln\left[\frac{R-y_F+3y_L}{R}\right] + \frac{R-y_F}{y_L}\ln\left[\frac{R-y_F}{R-y_F+y_L}\right]\right], & r \le R-y_F \end{cases} \tag{13}$$

2.3. Fracture

Fracture is strongly size-dependent, below which particles don't fracture upon lithiation, and above which particles initially form surface cracks due to lithiation-induced swelling (Liu et al., 2012). In order to probe this phenomenon, we analyzed several fracture models of electrodes (Wang et al., 2016). When the thickness of lithiation phase is less than 2 y_L, hoop stress is compressive, and thus a surface crack does not occur. When the thickness of lithiation phase is larger than 2 y_L and less than 3 y_L, the hoop stress on surface becomes tensile and then increases upto the yield strength σ_Y at the thickness larger than 3 y_L. Here it is worth noting that the crack propagation is assumed to be much faster than the plastic flow. Consequently, according to linear elastic fracture mechanics, the energy release rate, G_f, can be written as

$$G_f = Z\frac{\sigma_\theta^2}{E}R \tag{14}$$

where E is Young's modulus of electrode, and Z is a dimensionless parameter to be determined by solving the elastic boundary value problem.

Let us further assume that there is no volumetric change due to elastic or plastic deformation. Thus, the volumetric change can be represented as

$$\varepsilon_r + 2\varepsilon_\theta = \Omega c(r) \tag{15}$$

where $\varepsilon_r = \frac{du}{dr}$ is the radial strain, $\varepsilon_\theta = \frac{u}{r}$ is the hoop strain, and Ω is the volume per Li atom. For Si, the volume of a fully lithiated state swells by ~300%, so that $\Omega c_{max} = 3$. In addition, the phase boundary is

assumed fixed $u|_{R-y} = 0$. So the displacement is

$$u = \frac{3R}{2}\exp[-2r/R]\cdot\{-\exp[-2(R-y)/R] + \exp[2r/R]\} \tag{16}$$

The thickness of lithiation layer, t, can be described as

$$t = u_r|_{r=R} + y \tag{17}$$

Let Γ_f be the fracture energy and introduce the critical condition, $\Gamma_f = G_f$, for fracture initiation of electrode, we can obtain:

$$t = \frac{3R}{2}\left(1 - \exp\left[\frac{2y_L}{R}\left(1 + \sqrt{\frac{\Gamma_f E}{2\sigma_Y^2 R}}\right) - 4\right]\right) + y_L\left(1 + \sqrt{\frac{\Gamma_f E}{2\sigma_Y^2 R}}\right) \tag{18}$$

3. Results and discussion

As shown in Fig. 3, Li-ions gradually diffuse into the active material under the driving force of concentration gradient with a sharp phase boundary between lithiated and unlithiated phases. The bottom has the lowest concentration and finally reaches a maximum concentration c_0. Generally, lithiation involves two consequent processes: Li diffusion through the lithiated phase and chemical reaction at the two-phase boundary (see Fig. 1). There is a large solubility transition zone between these two phases, manifesting an abrupt change in Li concentration across the phase boundary.

Fig. 4 presents the stress $\sigma_\theta - \sigma_r$ as a piecewise function along the direction of radius. Similarly, there are three stress states: $y_F < y_L$ (solid line), $y_L < y_F < 3y_L$ (dashed line) and $3y_L < y_F$ (dotted line).

As shown in Fig. 5, it is obvious that the radial stress on surface is zero and is equal to the hoop stress in the unlithiated region. When the lithiated layer is very small, the stress state is tensile in the unlithiated region although the hoop stress on surface is compressive. This is because lithiated layer swelling drags the phase boundary to move outward and induces tension in the unlithiated layer. In the phase boundary, stress of the newly lithiated element is compressive owing to the constraint of surrounding materials. The element of phase boundary also extrudes the unlithiated region, causing to the stress transform from tension to compression in the unlithiated region.

It is seen in Fig. 6 that the similar trend of stress exists at different radial locations. The radial stress changes from tension to compression, and finally reaches a stable value. At the beginning of lithiated process, the Li-poor phase (element A in Fig. 2) is dragged by swelling the Li-rich phase (element C), causing the tensile stress of unlithiated materials. Owing to the constraint of surrounding materials, the newly lithiated element B suffers compressive stress, and finally plastic flow occurs. Also, the hoop stress state changes from tension to compression, and finally becomes stable. With the lithiated process, the stretch displacement in the hoop direction reaches a maximum value on surface under the stress state of $\sigma_\theta = \sigma_Y$. The stretch displacement of an inner element in the hoop direction decreases with the decrease of radius, but the inner element is still at the compressive state in the hoop direction even for full lithiation (e.g., $r = 0.8$ R).

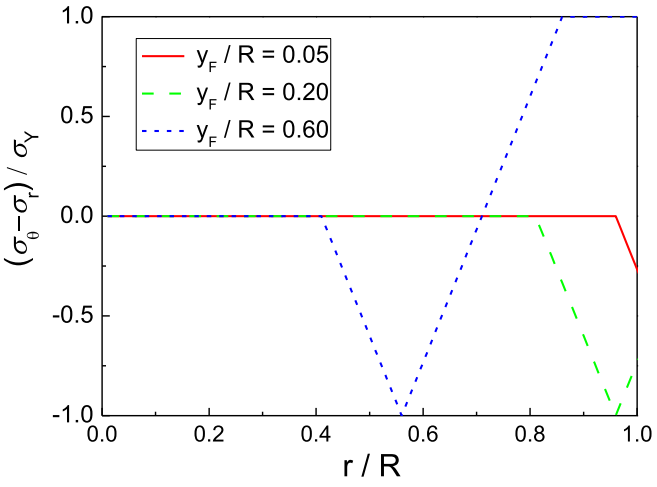

Fig. 4. Stress distributions of $\sigma_\theta - \sigma_r$ along the direction of radius.

As shown in Fig. 7, a smaller y_L means a sharper phase boundary, separating Li-poor from Li-rich phases. The stress evolution is the same as that for a small ratio of $y_L/R = 0.1$. While the transition layer increases, Li concentration distribution gradually increases following a single phase. For example, the hoop stress in the lithiated layer is always compressive for a big transition layer $y_F/R = 0.8$, which agrees well with the stress evolution of a single phase (Yao et al., 2011). Considering two neighboring material elements, the outer one always has higher Li concentration than its inner neighbor, which drives Li to flow inward. The concentration difference can result in expansion mismatch and accordingly an additional compressive hoop stress in the former.

Fig. 8 describes the critical condition of fracture at the first lithiation. The analytical solution predicts that, by using the fracture energy $\Gamma_f = 5.6$ J/m^2 (Pharr et al., 2013), the critical size is 64.4 nm, which is consistent with the experimental result of 75 nm (Liu et al., 2012). It is noted that, however, for a large size range up to 1000 nm, the critical size of t/R decreases with increasing R, due to the increase of surface hoop tensile stress during lithiation. More importantly, there is the critical lithiated thickness, below which particles neither crack nor fracture upon lithiation no matter how large their sizes. This is

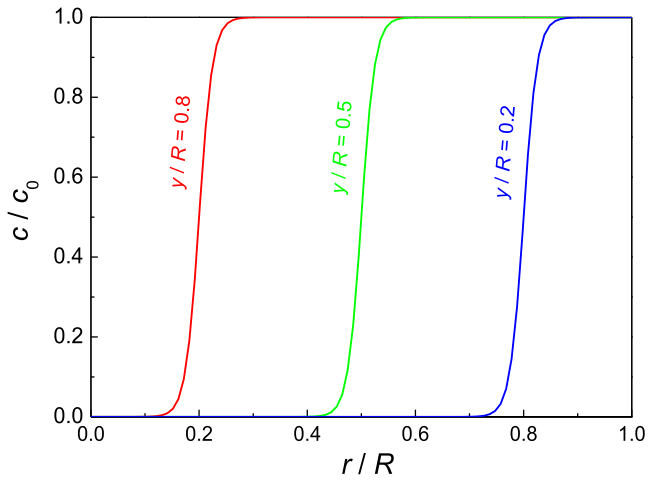

Fig. 3. Radial distributions of Li concentration under different lithiated states.

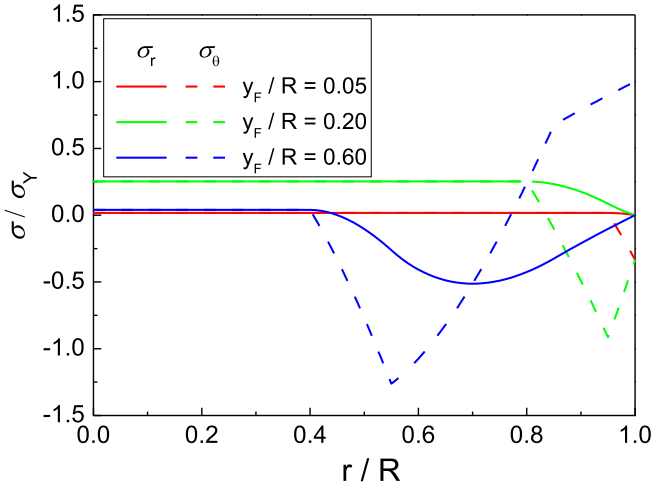

Fig. 5. Stress distributions of radial stress σ_r and hoop stress σ_θ.

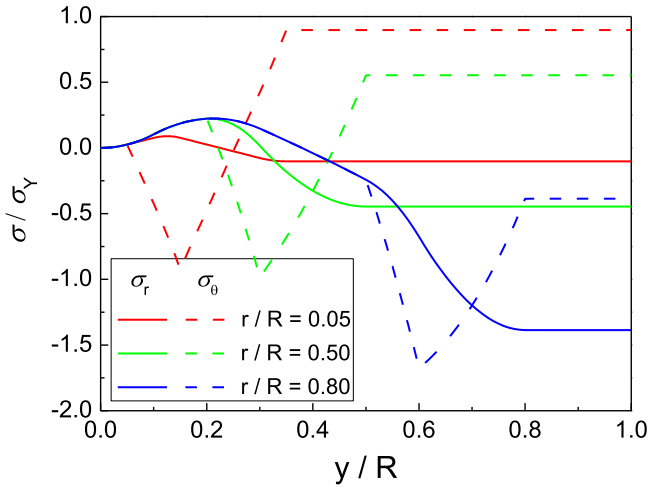

Fig. 6. The dependency of lithiated layer thickness on radial stress σ_r and hoop stress σ_θ.

attributed to the compressive hoop stress on surface at the beginning of lithiation.

In the lithiation process, the lithium ion concentration distributions can be divided into three parts, viz. poor-lithium layer, transition layer and rich-lithium layer. We assume that $\sigma_\theta - \sigma_r = 0$ in the poor-lithium layer, $\sigma_\theta - \sigma_r = \sigma_Y$ in the rich-lithium layer and an elastic transition layer between these two regions.

Based on the Taylor expansion, in the transition layer, Eq. (1) ($r \approx R - y$) can be simplified as:

$$\frac{c(r)}{c_0} \approx \frac{1}{1+1-\beta\frac{r-(R-y)}{R}} \approx \frac{1}{4}\beta\frac{r-(R-y)}{R} \tag{19}$$

Considering the elastic state, we have

$$\varepsilon_{ij} = \frac{1}{E}[(1+\nu)\sigma_{ij} - \nu\sigma_{ij}\delta_{ij}] + \frac{\Omega c(r)}{3}\delta_{ij} \tag{20}$$

According to the continuity and balance equations, the solution can be observed:

$$u = \frac{Ar}{2} + \frac{\Omega}{36}\frac{1+\nu}{1-\nu}\frac{\beta}{R}r^2 + \frac{B}{r} \tag{21}$$

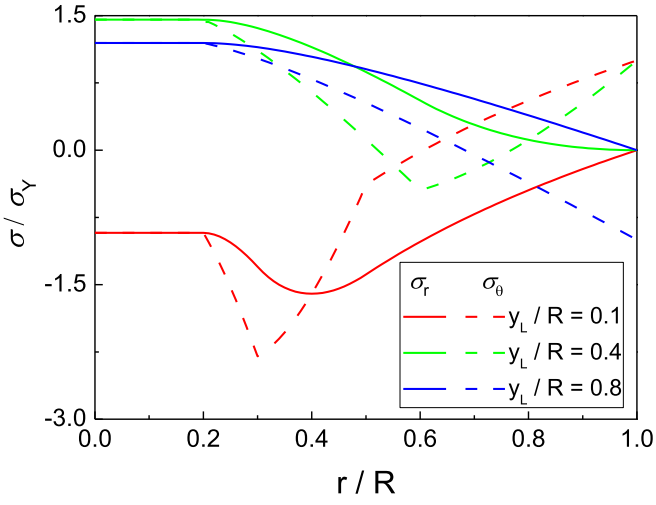

Fig. 7. The dependency of transition layer thickness on radial stress σ_r and hoop stress σ_θ.

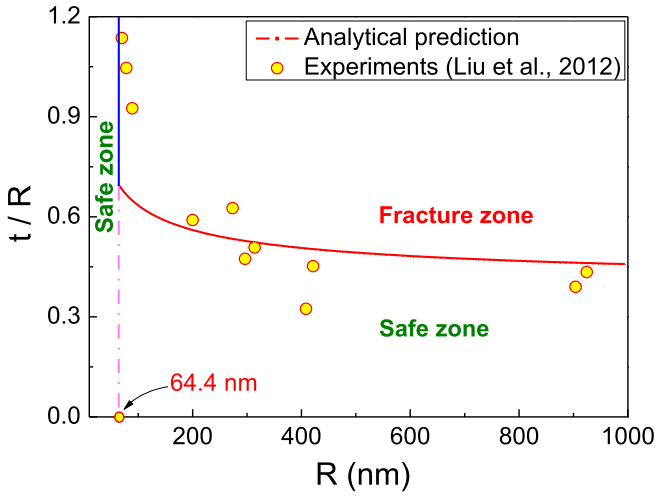

Fig. 8. Critical size of fracture for a spherical electrode.

$$\sigma_r - \sigma_\theta = \frac{E\left(-6f + \frac{\Omega}{3}\frac{1+\nu}{1-\nu}\frac{\beta}{4R}r^3\right)}{3r^2(1+\nu)} \tag{22}$$

here, A and B are undetermined parameters.

At $r = a$ (the position is the interface between poor-lithium layer and transition layer), $\sigma_r - \sigma_\theta = 0$,

$$f = \frac{a^3 A}{6} \tag{23}$$

$$\sigma_r - \sigma_\theta = \frac{-Ea^3}{36r^2}\frac{\Omega}{1-\nu}\frac{\beta}{R} + \frac{Er}{36}\frac{\Omega}{1-\nu}\frac{\beta}{R} \tag{24}$$

$$\frac{d(\widetilde{\sigma_r} - \widetilde{\sigma_\theta})}{dr} = \frac{E\Omega}{\sigma_Y(1-\nu)}\left(\frac{2a^3}{9r^3} + \frac{1}{9}\right)\frac{d\widetilde{c(r)}}{dr} \tag{25}$$

Because the transition layer is very thin, so $r \approx a$, and $E = 0.05\ \sigma_Y$ (Huang et al., 2013), Ω= 0.58 (Chen et al., 2014), so

$$\frac{20\times 0.58}{(1-0.22)\times 9}\frac{d\widetilde{c(r)}}{dr} < \frac{d(\widetilde{\sigma_r} - \widetilde{\sigma_\theta})}{dr} < \frac{3\times 20\times 0.58}{(1-0.22)\times 9}\frac{d\widetilde{c(r)}}{dr} \tag{26}$$

In this paper, we adopt $\frac{d(\widetilde{\sigma_r} - \widetilde{\sigma_\theta})}{dr} = 2\frac{d\widetilde{c(r)}}{dr}$, hence, the elastic transition layer is twice of concentration transition layer. The analytical solutions and numerical simulations of stress distributions are shown in Fig. 9. In the tendency of stress evolution, the analytical solutions are consistent with the results of numerical simulation. Thus, the correctness of present model has been verified by the J_2 model (Huang et al., 2013). Also, the neat linear assumption on the transition of stress layer has been shown in Fig. 2.

The lithiation process during charge and discharge is a very complicated and non-linear multi-physics process. However, most of the current investigations for stress evolutions at the two-phase boundary in high-capacity electroded of lithium-ion batteries are based on experimental observations and/or finite element simulations. For instance, the stresses in the amorphous layer were measured *in situ* during lithiation and delithiation processes (Chon et al., 2011); The phase-field models and finite element simulations were also applied to describe the Li-ion concentration distributions and the stress evolution (Pharr et al., 2012; Chen et al., 2014; Xie et al., 2016). Comparing with these former investigations, we firstly obtained the analytical solutions of stress evolutions at two-phase boundary. The analytical solutions avoid complicated formula derivation and unintuitive numerical calculation. Moreover, the results in this paper can be used to predict the surface cracks of lithiated particles with different sizes.

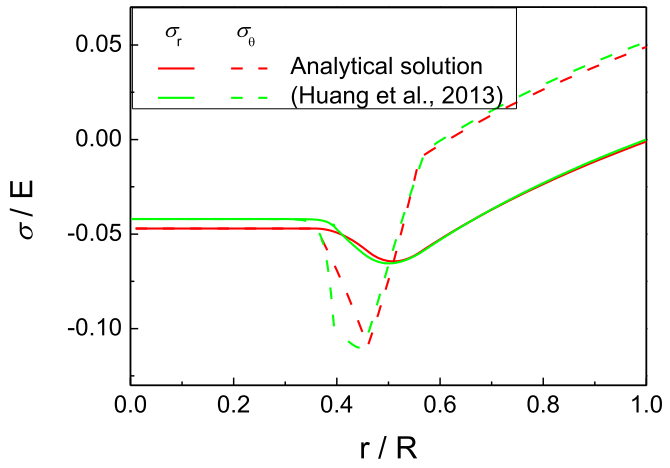

Fig. 9. The comparison between analytical solutions and numerical simulations of stress distributions.

4. Conclusions

In summary, we adopted a flexible sigmoid function together with a transition layer to characterize the stress state due to electrochemical reaction in LIBs. The analytical solution of stresses can be obtained based on an elastic-plastic model. It is shown that, when the transition layer is small, the stress evolution follows the two-phase mechanism because the hoop compressive stress becomes tension in the surface layer; otherwise, the hoop stress is always compressive for the big transition layer of a single-phase. Finally, by using the stress evolution and energy principle, analytical relation between the lithiated layer thickness and critical radius is obtained. Moreover, the critical thickness of lithiation phase is 2 y_L, below which particles neither crack nor fracture upon lithiation due to the compressive hoop stress.

Acknowledgments

This work was supported by the National Natural Science Foundation of China (Grant Nos. 11372267, 11402086 and 11472141).

References

Chan, C.K., Peng, H., Liu, G., McIlwrath, K., Zhang, X.F., Huggins, R.A., Cui, Y., 2008. High-performance lithium battery anodes using silicon nanowires. Nat. Nanotechnol. 3, 31–35.
Chen, L., Fan, F., Hong, L., Chen, J., Ji, Y., Zhang, S., Zhu, T., Chen, L., 2014. A phase-field model coupled with large elasto-plastic deformation: application to lithiated silicon electrodes. J. Electrochem. Soc. 161, F3164–F3172.
Chon, M.J., Sethuraman, V.A., McCormick, A., Srinivasan, V., Guduru, P.R., 2011. Real-time measurement of stress and damage evolution during initial lithiation of crystalline silicon. Phys. Rev. Lett. 107 045503.
Cui, Z., Gao, F., Qu, J., 2012. A finite deformation stress-dependent chemical potential and its applications to lithium ion batteries. J. Mech. Phys. Solid. 60, 1280–1295.
Haftbaradaran, H., Gao, H., 2012. Ratcheting of silicon island electrodes on substrate due to cyclic intercalation. Appl. Phys. Lett. 100 121907.
Huang, S., Fan, F., Li, J., Zhang, S., Zhu, T., 2013. Stress generation during lithiation of high-capacity electrode particles in lithium ion batteries. Acta Mater. 61, 4354–4364.
Jia, Z., Li, T., 2016. Intrinsic stress mitigation via elastic softening during two-step electrochemical lithiation of amorphous silicon. J. Mech. Phys. Solid. 91, 278–290.
Lee, S., Wang, W., Chen, J., 2000. Diffusion-induced stresses in a hollow cylinder. Mater. Sci. Eng., A 285, 186–194.
Liu, X.H., Zheng, H., Zhong, L., Huang, S., Karki, K., Zhang, L.Q., Liu, Y., Kushima, A., Liang, W.T., Wang, J.W., Cho, J.H., Epstein, E., Dayeh, S.A., Picraux, S.T., Zhu, T., Li, J., Sullivan, J.P., Cumings, J., Wang, C., Mao, S.X., Ye, Z.Z., Zhang, S., Huang, J.Y., 2011. Anisotropic swelling and fracture of silicon nanowires during lithiation. Nano Lett. 11, 3312–3318.
Liu, X.H., Zhong, L., Huang, S., Mao, S.X., Zhu, T., Huang, J.Y., 2012. Size-dependent fracture of silicon nanoparticles during lithiation. ACS Nano 6, 1522–1531.
Ma, Z., Li, T., Huang, Y.L., Liu, J., Zhou, Y., Xue, D., 2013. Critical silicon-anode size for averting lithiation-induced mechanical failure of lithium-ion batteries. RSC Adv. 3, 7398–7402.
Ma, Z., Xie, Z., Wang, Y., Zhang, P., Pan, Y., Zhou, Y., Lu, C., 2015. Failure modes of hollow core–shell structural active materials during the lithiation–delithiation process. J. Power Sources 290, 114–122.
McDowell, M.T., Lee, S.W., Harris, J.T., Korgel, B.A., Wang, C., Nix, W.D., Cui, Y., 2013. In situ TEM of two-phase lithiation of amorphous silicon nanospheres. Nano Lett. 13, 758–764.
McDowell, M.T., Lee, S.W., Wang, C., Nix, W.D., Cui, Y., 2012. Studying the kinetics of crystalline silicon nanoparticle lithiation with in situ transmission electron microscopy. Adv. Mater. 24, 6034–6041.
Mukhopadhyay, A., Sheldon, B.W., 2014. Deformation and stress in electrode materials for Li-ion batteries. Prog. Mater. Sci. 63, 58–116.
Nam, K.T., Kim, D.W., Yoo, P.J., Chiang, C.Y., Meethong, N., Hammond, P.T., Chiang, Y.-M., Belcher, A.M., 2006. Virus-enabled synthesis and assembly of nanowires for lithium ion battery electrodes. Science 312, 885–888.
Pharr, M., Suo, Z., Vlassak, J.J., 2013. Measurements of the fracture energy of lithiated silicon electrodes of Li-ion batteries. Nano Lett. 13, 5570–5577.
Pharr, M., Zhao, K., Wang, X., Suo, Z., Vlassak, J.J., 2012. Kinetics of initial lithiation of crystalline silicon electrodes of lithium-ion batteries. Nano Lett. 12, 5039–5047.
Prussin, S., 1961. Generation and distribution of dislocations by solute diffusion. J. Appl. Phys. 32, 1876–1881.
Sethuraman, V.A., Chon, M.J., Shimshak, M., Srinivasan, V., Guduru, P.R., 2010. In situ measurements of stress evolution in silicon thin films during electrochemical lithiation and delithiation. J. Power Sources 195, 5062–5066.
Song, Y., Lu, B., Ji, X., Zhang, J., 2012. Diffusion induced stresses in cylindrical lithium-ion batteries: analytical solutions and design insights. J. Electrochem. Soc. 159, A2060–A2068.
Takamura, T., Ohara, S., Uehara, M., Suzuki, J., Sekine, K., 2004. A vacuum deposited Si film having a Li extraction capacity over 2000 mAh/g with a long cycle life. J. Power Sources 129, 96–100.
Van Noorden, R., 2014. The rechargeable revolution: a better battery. Nature 507, 26–28.
Wada, T., Ichitsubo, T., Yubuta, K., Segawa, H., Yoshida, H., Kato, H., 2014. Bulk-nanoporous-silicon negative electrode with extremely high cyclability for lithium-ion batteries prepared using a top-down process. Nano Lett. 14, 4505–4510.
Wang, C., Ma, Z., Wang, Y., Lu, C., 2016. Failure prediction of high-capacity electrode materials in lithium-ion batteries. J. Electrochem. Soc. 163, A1157–A1163.
Wang, J.W., He, Y., Fan, F., Liu, X.H., Xia, S., Liu, Y., Harris, C.T., Li, H., Huang, J.Y., Mao, S.X., 2013. Two-phase electrochemical lithiation in amorphous silicon. Nano Lett. 13, 709–715.
Xie, Z., Ma, Z., Wang, Y., Zhou, Y., Lu, C., 2016. A kinetic model for diffusion and chemical reaction of silicon anode lithiation in lithium ion batteries. RSC Adv. 6, 22383–22388.
Yang, F., 2011. Criterion for insertion-induced microcracking and debonding of thin films. J. Power Sources 196, 465–469.
Yang, F., 2013. Effect of diffusion-induced bending on diffusion-induced stress near the end faces of an elastic hollow cylinder. Mech. Res. Commun. 51, 72–77.
Yang, H., Huang, S., Huang, X., Fan, F., Liang, W., Liu, X.H., Chen, L.-Q., Huang, J.Y., Li, J., Zhu, T., 2012. Orientation-dependent interfacial mobility governs the anisotropic swelling in lithiated silicon nanowires. Nano Lett. 12, 1953–1958.
Yao, Y., McDowell, M.T., Ryu, I., Wu, H., Liu, N., Hu, L., Nix, W.D., Cui, Y., 2011. Interconnected silicon hollow nanospheres for lithium-ion battery anodes with long cycle life. Nano Lett. 11, 2949–2954.
Zhao, K., Pharr, M., Hartle, L., Vlassak, J.J., Suo, Z., 2012a. Fracture and debonding in lithium-ion batteries with electrodes of hollow core–shell nanostructures. J. Power Sources 218, 6–14.
Zhao, K., Pharr, M., Vlassak, J.J., Suo, Z., 2010. Fracture of electrodes in lithium-ion batteries caused by fast charging. J. Appl. Phys. 108 073517.
Zhao, K., Pharr, M., Wan, Q., Wang, W.L., Kaxiras, E., Vlassak, J.J., Suo, Z., 2012b. Concurrent reaction and plasticity during initial lithiation of crystalline silicon in lithium-ion batteries. J. Electrochem. Soc. 159, A238–A243.
Zhao, K., Wang, W.L., Gregoire, J., Pharr, M., Suo, Z., Vlassak, J.J., Kaxiras, E., 2011. Lithium-assisted plastic deformation of silicon electrodes in lithium-ion batteries: a first-principles theoretical study. Nano Lett. 11, 2962–2967.